Stochastic Algorithms for the Analysis of Numerical Flame Simulations

John B. Bell, Marcus S. Day, Joseph F. Grcar and Michael J. Lijewski

Center for Computational Sciences and Engineering
Lawrence Berkeley National Laboratory
Berkeley, California, 94720, USA

April, 2004

Abstract

Recent progress in simulation methodologies and high-performance parallel computers have made it is possible to perform detailed simulations of multidimensional reacting flow phenomena using comprehensive kinetics mechanisms. As simulations become larger and more complex, it becomes increasingly difficult to extract useful information from the numerical solution, particularly regarding the interactions of the chemical reaction and diffusion processes. In this paper we present a new diagnostic tool for analysis of numerical simulations of reacting flow. Our approach is based on recasting an Eulerian flow solution in a Lagrangian frame. Unlike a conventional Lagrangian viewpoint that follows the evolution of a volume of the fluid, we instead follow specific chemical elements, e.g., carbon, nitrogen, etc., as they move through the system. From this perspective an "atom" is part of some molecule of a species that is transported through the domain by advection and diffusion. Reactions cause the atom to shift from one chemical host species to another and the subsequent transport of the atom is given by the movement of the new species. We represent these processes using a stochastic particle formulation that treats advection deterministically and models diffusion and chemistry as stochastic processes. In this paper, we discuss the numerical issues in detail and demonstrate that an ensemble of stochastic trajectories can accurately capture key features of the continuum solution. The capabilities of this diagnostic are then demonstrated by applications to study the modulation of carbon chemistry during a vortex-flame interaction, and the role of cyano chemistry in NO_x production for a steady diffusion flame.

1 Introduction

Advances in simulation methodologies and high-performance computers make feasible detailed simulations of multidimensional reacting flow phenomena using comprehensive reaction sets [21]. For steady flames, Smooke and his co-workers [6, 10, 26, 32–35] have performed numerous studies of laminar methane diffusion flames with detailed kinetics. Mechanisms that include detailed nitrogen chemistry were used by Bell and colleagues [4, 19, 36] to study NO_x chemistry in ammonia-enriched methane flames. For transient laminar flames, Hilka et al. [22], Najm and co-workers [27–29], and Bell et al. [2], studied vortex-flame interactions with detailed methane chemistry. For premixed flames in fields of two-dimensional (2D) isotropic turbulence, Baum et al. [1] studied turbulence-flame interactions with detailed hydrogen chemistry, Haworth et al. [20] studied the effects of mixture inhomogeneity with a detailed propane mechanism, Chen and Im [7] considered local flame speed using detailed methane chemistry, and Echekki and Chen [9] studied autoignition with a detailed hydrogen mechanism. Vervisch et al. [42] studied a 2D turbulent premixed V-flame with detailed hydrogen chemistry. For 3D simulations with detailed hydrogen chemistry, Tanahashi et al. [37, 38] examined turbulent premixed flame sheets, Mizobuchi et al. [25] determined the structure of turbulent jet diffusion flames, and Tsuboi et al. [41] predicted diagonal structures in turbulent detonation fronts. For 3D simulations with detailed methane chemistry, Bell et al. [3, 5] studied turbulent premixed flame sheets and laboratory-scale turbulent V-flames. Complex reaction systems are also used to model nuclear burning in simulations of supernovae: for example see Timmes and Woosley [39], Timmes et al. [40] and Fryxell et al. [12].

The scientific utility of these simulations depends on the ability to analyze the implications of what is computed and to draw conclusions about the underlying chemical kinetics [13]. As the simulations grow in complexity this task becomes increasingly difficult. For example, one-dimensional calculations show [18] the relationship between preheat and heat-release zones in premixed laminar flames, but for turbulent flames probability distributions are needed just to tabulate the range of chemical states. The close coupling between advection, diffusion and chemical kinetics in time-dependent turbulent systems makes analysis difficult even in the simplest settings.

In this paper, we develop a diagnostic tool for analyzing multi-component, multi-dimensional reacting flow problems with detailed kinetics. We intend the analysis to be undertaken after a continuum calculation has been performed. Thus we assume the distribution of all species as well as the temperature and velocity fields over all space and time are known. Our analysis procedure then interrogates the solution by following "particles" that track one of the specific kinds of atoms in the chemical species comprising the fluid. For example, to understand basic flame chemistry in a hydrocarbon flame we might track the behavior of carbon atoms; to study NO_x formation we might track nitrogen atoms. We not only follow the particles as they traverse paths in the flow (analogous to tracing the evolution of passive particles in a flow field), we must also account for the effects of differential diffusion and chemical reactions. We approximate diffusion as a random walk whose probability of making a step is determined by the local diffusivity of the host species. Chemical reactions, which transfer the traced atom from one species to another, are approximated as a Markov process whose transitions are determined from the elementary steps of the reaction mechanism. Statistics from tracing an ensemble of such stochastic particles are collected and used to analyze the interplay of convection, diffusion, and reaction in the flame.

After introducing the method in the next section, we will demonstrate the utility of this new approach for several prototype problems. First, we will relate stochastically obtained diagnostics to more conventional characteristics of the flame derivable from the continuum solution. In doing so, we can quantify statistical requirements and validate the diagnostics. In addition, we present two more interesting applications of the diagnostics: the modulation of carbon chemistry in a premixed

methane flame interacting with a vortex, and the role of cyano chemistry on NO_x formation in a methane diffusion flame. In each case we demonstrate that the stochastic particle diagnostics allow us to pose complex analysis questions in a straightforward manner and provide interesting insights into the flow.

2   Diagnostic Algorithm

The basic idea for the diagnostic algorithm is to monitor the path of a tagged atom (or collection of atoms) through the flow domain, including the history of which molecules transport them. The data to be analyzed includes the distribution of all species in the continuum solution, as well as the temperature and velocity fields. This data is obtained through numerical simulation of the reacting Navier-Stokes equations. Our analysis is independent of whether the solution is obtained with a compressible or low Mach number formulation, but does depend on the details of the transport and kinetics models employed. To focus the exposition, we assume that the numerical simulations that we wish to analyze (and, consequently the diagnostic algorithm as well) are based on a mixture-averaged model for transport and a collection of fundamental reactions specified as a CHEMKIN [24] compatible kinetics database. With these assumptions, the k-th species satisfies the equation

$$\frac{\partial \rho Y_k}{\partial t} + \nabla \cdot (u \rho Y_k) \;=\; \rho \frac{DY_k}{Dt} \;=\; \nabla \cdot \rho D_k \nabla Y_k + \rho \omega_k \,, \tag{1}$$

where Y_k is the mass fraction, ρ is fluid density, u is advection velocity, and D_k and ω_k are the mixture-averaged diffusion coefficient and chemical production rate, respectively. We note that it would be a simple matter to tailor the analysis to other, similar, models as appropriate.

We are interested in following atoms of some specific element such as carbon or nitrogen as they propagate through the system. We denote the atom we are tracking by A. For the chemical system being modeled there is a subset of the molecules, $M_1, M_2, \ldots, M_K$ that contain atoms of the type A as one of their constituents. At each time, the atom A is thus in one of the elements, M_k, which we denote by $A \in M_k$. If we specify a probability distribution that determines how A is initially dispersed throughout the system, equation (1) prescribes the evolution of that distribution.

If we interpret the species equation from the perspective of an atom, $A \in M_k$, we obtain a stochastic differential equation for the fate of the particle in the flow field:

$$dx_A \;=\; u(x_A, t)dt + dW_{k(t)}(x_A, t) + dR_{k:k'}(x_A, t) \,, \tag{2}$$

where the terms on the right hand side represent advection, diffusion and reaction. In particular, $u(x_A, t)$ is the velocity obtained from the continuum solution, and $dW_{k(t)}$ represents a generalized Brownian motion with properties chosen to model the diffusion of the M_k molecules. Finally, $dR_{k:k'}$ denotes a "scattering" of A from M_k into the set $M_{k'}$ as the result of reaction. After M_k reacts, the dynamics of the particle are determined by the motion of the k'-th species. We integrate equation (2) over a time interval, Δt, using a time-explicit split approach that treats each term independently.

The first term in equation (2) corresponds to a standard particle tracing algorithm and requires no elaboration. We want to represent diffusion as a random walk; however, rather than attempting to construct an analytic form of the random walk to model species diffusion, we introduce a spatial scale Δx and a temporal scale Δt and use a lattice model to approximate the random walk. In particular, we consider the standard time-explicit one-dimensional centered discretization of the diffusion term in equation (1). At three adjacent lattice points we have

$$\rho Y_{k,j-1}^{n+1} \;=\; \rho Y_{k,j-1}^{n} + \frac{\Delta t}{\Delta x^2} \left[(\rho D)_{k,j-\frac{1}{2}}^{n} (Y_{k,j}^{n} - Y_{k,j-1}^{n}) - (\rho D)_{k,j-\frac{3}{2}}^{n} (Y_{k,j-1}^{n} - Y_{k,j-2}^{n}) \right] \,,$$

$$\rho Y_{k,j}^{n+1} = \rho Y_{k,j}^{n} + \frac{\Delta t}{\Delta x^2}\left[(\rho D)_{k,j+\frac{1}{2}}^{n}(Y_{k,j+1}^{n} - Y_{k,j}^{n}) - (\rho D)_{k,j-\frac{1}{2}}^{n}(Y_{k,j}^{n} - Y_{k,j-1}^{n})\right],$$

$$\rho Y_{k,j+1}^{n+1} = \rho Y_{k,j+1}^{n} + \frac{\Delta t}{\Delta x^2}\left[(\rho D)_{k,j+\frac{3}{2}}^{n}(Y_{k,j+2}^{n} - Y_{k,j+1}^{n}) - (\rho D)_{k,j+\frac{1}{2}}^{n}(Y_{k,j+1}^{n} - Y_{k,j}^{n})\right].$$

Here, the j-subscript represents a lattice location. Subscripts $j\pm 1$ represents locations immediately to the right or left, separated by a distance Δx. If we start with a mass, ρY_k at x_j and time t^n, then at $t^n + \Delta t$, the fraction $p_R = \Delta t(\rho D)_{k,j+\frac{1}{2}}^{n}/\Delta x^2$ of that mass moves to the right a distance Δx, and the fraction $p_L = \Delta t(\rho D)_{k,j-\frac{1}{2}}^{n}/\Delta x^2$ moves to the left. The remaining mass stays at its original location.

For Δt sufficiently small that $p_R + p_L < 1$, these expressions define a discrete probability distribution that approximates the diffusion of molecules, M_k. The path x_A^n of a trace particle associated with a molecule M_k at time t^n over the time interval Δt, is computed according to the following prescription. We first perform an advective update of the particle location to obtain $x_A^* = x_A^n + \Delta t\, u$. We then choose a random number $\alpha \in [0,1]$ and define the diffusion update as the random-walk step:

$$x_A^{n+1} = \begin{cases} x_A^* + \Delta x & \text{if } 0 \leq \alpha \leq p_R, \\ x_A^* - \Delta x & \text{if } p_R < \alpha \leq p_R + p_L, \\ x_A^* & \text{if } p_R + p_L < \alpha \leq 1. \end{cases}$$

For $\Delta t\, D_{max}/\Delta x^2 \ll 1$ this lattice approximation provides sufficient accuracy that statistical sampling error dominates errors arising from the lattice approximation. The generalization of this approach to two and three space dimension is straightforward. Based on tests for model problems, we have estimated that setting Δt as 10% of the local stability limit of the explicit diffusion scheme provides an suitable balance between accuracy and efficiency.

Our approach to modeling the chemical reaction terms in equation (2) is based on a similar type of discrete time approximation to the underlying stochastic process. To that end, we introduce a time interval Δt_c over which we wish to model the chemistry. We note that the chemical time scale depends on the particular molecule we are considering and its local environment. Thus, the computation of Δt_c is based on local considerations. If $A \in M_k$ at t^n, there are a collection of reactions, $r_1, \ldots, r_N$, that transform M_k, along with other reaction participants, into a new collection of molecules over the time interval, Δt_c. As a result of this transformation M_k is destroyed and A is transferred from a molecule of type M_k to one of type $M_{k'}$. This destruction of M_k is expressed at the continuum level as

$$\frac{d[M_k]}{dt} = -\sum_{n=1}^{N} R_n. \tag{3}$$

where $[M_k]$ is the molar concentration of M_k, and R_n is the rate of progress of reaction, r_n, destroying molecules of type M_k. Reactions representing creation of M_k are not considered because these reactions do not affect A. Assuming Δt_c is sufficiently small, (3) can be approximated by

$$[M_k]^{n+1} = [M_k]^n(1 - \Delta t_c \sum_{n=1}^{N} R_n/[M_k]),$$

so we can define $p_n = \Delta t_c R_n/[M_k]$ to be the probability that reaction r_n transforms A from M_k to $M_{k'}$ during the time interval Δt_c. We also define $p_0 = (1 - \Delta t_c \sum_{n=1}^{N} R_n/[M_k]) > 0$ as the probability that the molecule M_k containing A does not react during the time interval.

The representation of the kinetics is constructed so that probabilities of reaction depend only on the current state; thus, the probabilistic model for the transfer of A from molecule to molecule as a result of reactions is a Markov process $\mathfrak{M}$. A simple graphical illustration of this type of process is shown in Figure 1. As with the diffusion, we specify Δt_c as a fraction of the maximum stable explicit time step, namely, 10% of the maximum value of Δt_c for which $p_0 > 0$. We note that the time scale associated with the reaction kinetics is typically much smaller than the diffusion and advection time scales. Thus, we subcycle the chemistry as necessary until we have modeled the process over the full interval Δt.
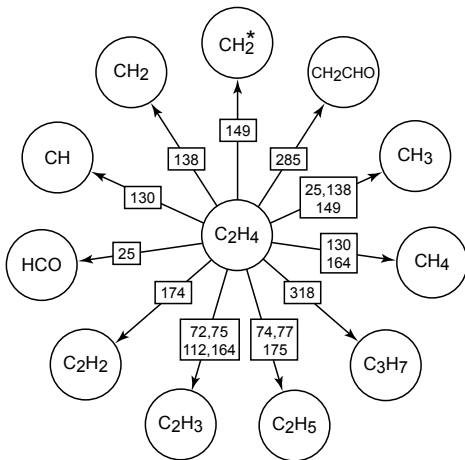
Figure 1: State-transition diagram for ethylene, including numbered reactions from the GRI-Mech 3.0 kinetics mechanism [11], illustrating the chemical reactions that shift carbon atoms to other molecules.

There are several subtleties that must be addressed in construction of $\mathfrak{M}$ to correctly represent the chemical behavior and to satisfy the Markov property. Particular issues relate to (i) fast, near equilibrium reactions, (ii) detail of the behavior of specific reactions, and (iii) molecules with multiple copies of the same atom. These issues are discussed in the Appendix.

This completes the basic description of the algorithm. In summary, to analyze a particular feature of a simulation, we identify the type of atom we want to follow, the initial molecule of which it is a constituent and the region in space and time where we want to begin the trajectories. This data is used to initialize an ensemble of particles that are evolved by the stochastic algorithm described above. Namely, we first identify Δt for the transport calculation. We then compute the deterministic advection of the particle followed by the random walk to represent diffusion. We then choose Δt_c and advance the chemistry, subcycling as necessary, until we reach Δt. For time dependent flows, we have approximated the data for a given time step as piecewise constant over the length of the time step of the fluid dynamics algorithm; i.e., we assume the data obtained from the fluid solution at time t^n is valid until time t^{n+1} which is the time at which the next fluid time step is available. We adjust Δt for the stochastic particle algorithm so that the diagnostic algorithm reaches t^{n+1} exactly and we compute new properties to continue the evolution. We then interrogate the collected trajectories to analyze the behavior of the flow.

Before illustrating the performance of the method we first make a couple of observations about the method. At first examination it would appear that the computations are quite costly. However, most of the required data can be precomputed, so that the actual particle integration is quite

efficient. Also, since each trajectory is independent, the method parallelizes very well. Exploiting these characteristics of the method, we have been able to follow a several hundred thousand trajectories in just a few hours.

A second observation about this approach is a word of caution. With the stochastic description of the algorithm it is tempting to try to relate the stochastic particles to a Boltzmann description of the fluid. However, unlike a Boltzmann description we do not maintain velocity distribution for the particles. Thus, our particles represent, at best, "pseudo-particles" whose velocities are averages of the Boltzmann velocity description. Perhaps the most accurate description of an ensemble of stochastic trajectories is as a path integral representation of an approximation to the continuum solution.

3   Computational Results

In this section we demonstrate the behavior of the method and illustrate the relationship between the particle trajectories and the continuum solution. We consider two examples, premixed flames and laminar diffusion flames. Both examples use detailed methane chemistry and a mixture model for diffusion. The sample flames were computed using the low Mach number adaptive mesh refinement algorithm developed by Day and Bell [8].

3.1   Steady Premixed Methane Flame

In this subsection, we demonstrate the application of the stochastic particle algorithm to premixed flames. We first apply the method to a steady premixed flame in order to validate the algorithm. The steady laminar flame solution at fuel equivalence ratio $\phi = 1.2$ was computed with the PREMIX code [23] that is part of CHEMKIN application suite using the supplied model for mixture-averaged diffusion. The GRI-Mech 3.0 [11] database was used for all kinetics, thermodynamic and transport parameters.

We map this one-dimensional solution onto a locally-refined two-dimensional domain with inflowing reactants and the bottom and products exiting at the top by replicating the solution horizontally. We track 80,000 particles representing carbon atoms that are initially part of the CH_4 molecules. The particles are "released" near the bottom of the domain and allowed to propagate upward through the system. Trajectories for six sample particles are shown in Figure 2. Since there is no horizontal advection, all lateral motion results from the random walk algorithm describing diffusion. Red indicates the path taken in physical space while the traced carbon atom resides in a CH_4 molecule. The portion of the path alternating in color between blue and green represents the transfer the carbon atom between CO and CO_2 in the region downstream of the flame. The flame, corresponding to the location of peak heat release, is at $y = .02$ m.

Reaction pathway diagrams are a standard directed-graph approach used to analyze reacting fluid systems. Nodes in these graphs represent chemical species, and edges represent transformation from species to species by chemical reaction. To compile the analogous chemical behavior generated by the stochastic particles, we tabulate all of the chemical transformations taken in the Markov process representation of chemistry, coalesce all of the transformations representing different reactions that result in the same molecular transformation and compute the net transformation for each molecular pathway. This data is represented graphically for the evolution of carbon atoms in Figure 3 along the with analogous diagram computed by integrating the net chemical production rates obtained from PREMIX over the computational domain. In these graphs, the thickness of the arrows is scaled by the relative strength of that pathway, normalized to the $CH_4 \rightarrow CH_3$ pathway which is the dominant path for carbon chemistry in methane oxidation. A detailed comparison of
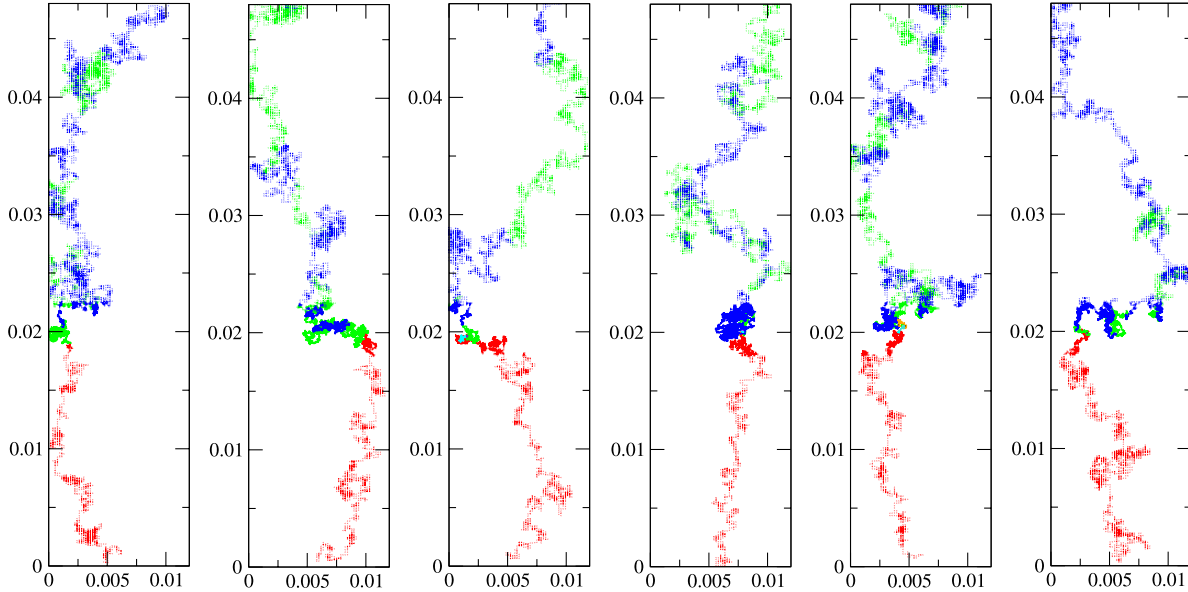
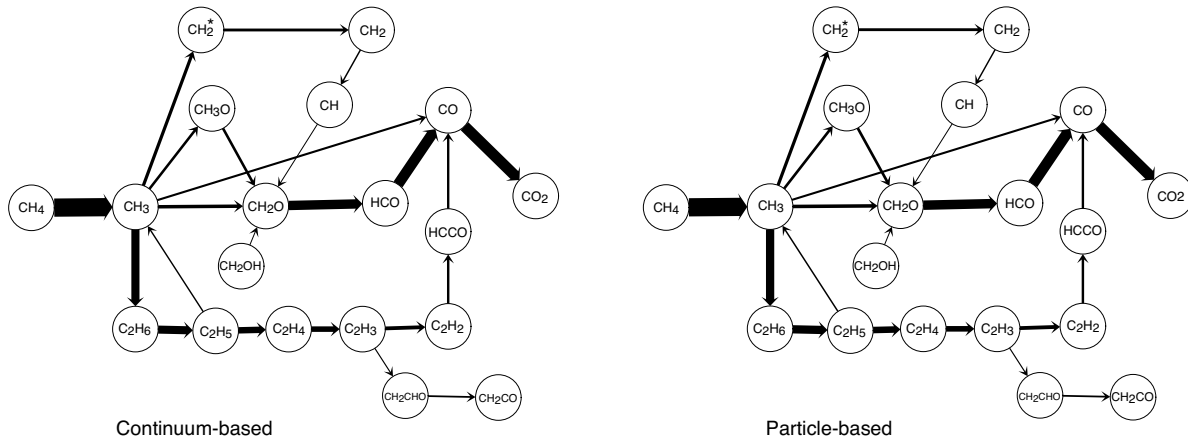Figure 2: Carbon trajectories for flat laminar premixed flame, $\phi = 1.2$

Figure 3: Reaction path diagrams for rich ($\phi = 1.2$) premixed methane flame computed using PREMIX with GRI-Mech 3.0: continuum-based CHEMKIN rate evaluation, and particle-based tabulation of 80,000 trajectories.

the data shows that the stochastic particle representation accurately captures the chemical behavior of the flame with errors of less than 1%.

3.2 Vortex-Flame Interactions

The next example addresses the interaction of a vortex with a premixed flame. This configuration has been studied computationally by a number of authors; see, for example, [2, 28, 29]. We begin with a flat premixed flame oriented normal to the inlet flow and superimpose a velocity field due to a periodic array of counter-rotating vortex pairs with Gaussian cores 2.25 mm wide and

centers 2.50 mm apart. These parameters produce a vortex pair that is similar in width and propagation speed to the vortex pair in described in the V-flame experiment as realized by Nguyen and Paul [30, 31]. A schematic for the computation is presented in Figure 4. From symmetry consider-
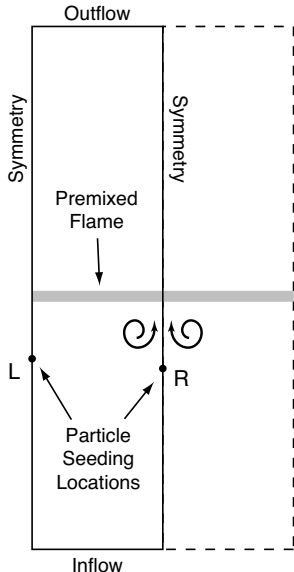

Figure 4: Schematic of the premixed methane flame-vortex problem. The shaded line represents the position of the flame, and the swirl lines represent the initial vortex. We impose symmetry along the sides of the 1.2×4.8 cm domain to avoid modeling the dotted region.

ations, we need only simulate one half of a period of the problem. Here we take the right boundary to correspond to the vortex centerline. Reactants flow in at the bottom, and combustion products exit through the top. For the conditions presented here, vortex pair propagates upward with a self-induced velocity of approximately 130 cm/s. We consider two equivalence ratios, $\phi = 0.8$ and 1.2. Our base computational domain is 1.2 cm wide, and 4.8 cm high with an effective resolution of 256×1024 corresponding to $\Delta x = 47\mu$ m at the finest level of resolution.

We simulate the lean flame ($\phi = 0.8$) until $t_f = 12$ ms, and the rich flame ($\phi = 1.2$) until $t_f = 22$ ms. For the cases considered, there are a number of interesting stoichiometry-dependent changes in the chemical behavior as the vortex interacts with the flame; we focus on two of them. First, in the rich case we observe a dramatic reduction in CH as the vortex interacts with the flame, similar to what was observed by Nguyen and Paul [30]. Second, for both equivalence ratios, we observe an enhancement in CH_3O as the flame is stretched by the vortex. Snapshots of the mole fraction of CH and CH_3O for each case are presented in Figure 5. Our goal is to apply the stochastic particle algorithm to the simulation data to understand the behavior of these two chemical species.

To analyze how the vortex interaction changes the flame chemistry, we want to compare the behavior of carbon atoms passing through the stretched portion of the flame to the behavior of carbon atoms passing through a relatively unperturbed portion of the flame. For this purpose we initialize 400,000 carbon particles, initially in CH_4, at the points labeled L and R in Figure 4 at initial time. These positions represent two locations at time $t = 0$ of fluid that will enter the flame at approximately 8 ms. For each starting location we then look at the subset of the stochastic paths for particles passing through the flame in a given space-time window, ignoring those with trajectories not relevant for analyzing CH behavior near the centerline.
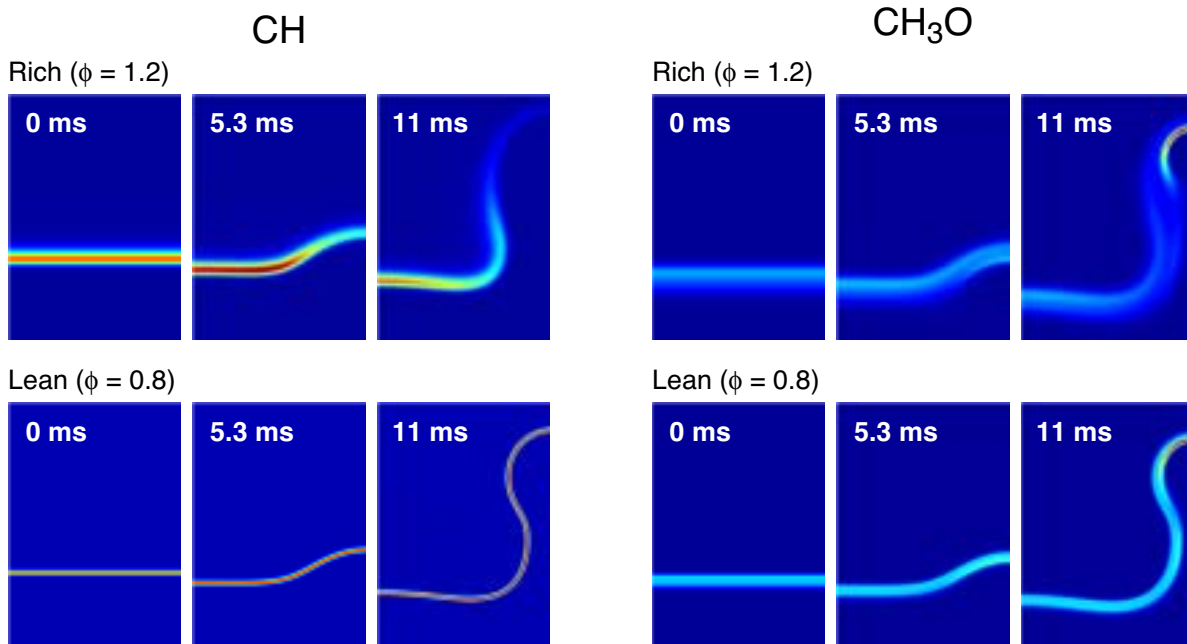
8

Figure 5: Behavior of CH and CH$_3$O during vortex flame interaction for $\phi = 0.8$ and 1.2

We compute reaction pathway diagrams as before for stretched (R) and unperturbed (L) sections of the flame by tabulating the chemical transformations in the stochastic particle trajectories. The lean case is shown in Figure 6 and the rich case is shown in Figure 7.

Comparing the reaction paths, we find that for the lean case, the interaction with the vortex induces minimal changes in the basic carbon chemical pathways, consistent with the behavior of CH observed in Figure 5. For the rich case, the vortex interaction leads to a dramatic shift in the chemical pathways. In particular, the data shows a marked shift away from the CH$_3$ $\rightarrow$ CH$_2$(s) pathway combined with an enhancement of the CH$_3$ $\rightarrow$ C$_2$H$_6$ pathway. This preferential shift toward the C_2 pathway is the major cause leading to the reduction in CH.

To explore the shifting of the chemical pathways in more detail, we analyze the reaction events in the stochastic particle trajectories that create and destroy CH$_3$. In Figure 8, CH$_3$ pathways are presented for both the left and right sides of the flame for the rich case. The CH$_3$ chemistry is dominated by a relatively small number of reactions—four reactions describing the CH$_4$ $\rightarrow$ CH$_3$ kinetics and the seven destruction reactions depicted in the figure. (Three of which are also significant in the reverse direction producing CH$_3$.) The pathways may be distinguished by whether they involve radical species as reaction partners. Those that involve radical species show a marked relative reduction on the strained side of the flame compared to those in the unperturbed flame. The remaining reactions, involving recombination or partnering with a stable chemical species show a corresponding increase. Additional particle statistics confirm that on the strained side of the flame, the reactions destroying CH$_3$ occur at lower concentrations of the relevant radical species.

From the above analysis, we see that to further explore this shift in chemical pathways, we need to examine the reduction in the radical pool. Classical stretched flame theory suggests that Lewis number effects, especially in the mobile H and H$_2$ molecules, are likely to impact the chemistry near the region of intense flame interaction with the vortex. To explore how the observed behavior is related to flow strain we generated an ensemble of particle trajectories for H atoms bound originally
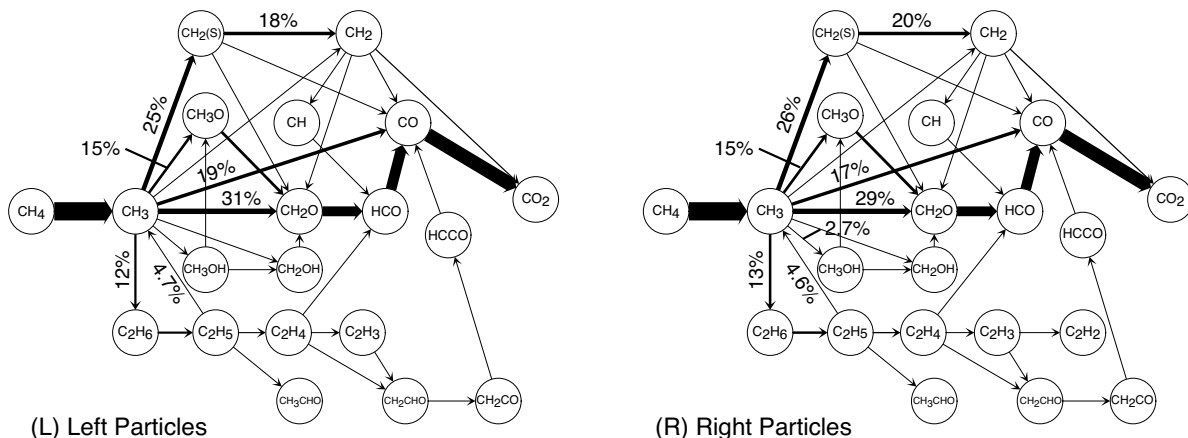
9

Figure 6: Carbon reaction path diagrams for vortex flame interaction, $\phi = 0.8$. Here only paths of strength $> 1\%$ of the largest path, $CH_4 \rightarrow CH_3$, are shown. For some paths of interest their weights are shown as a percent of the strongest.
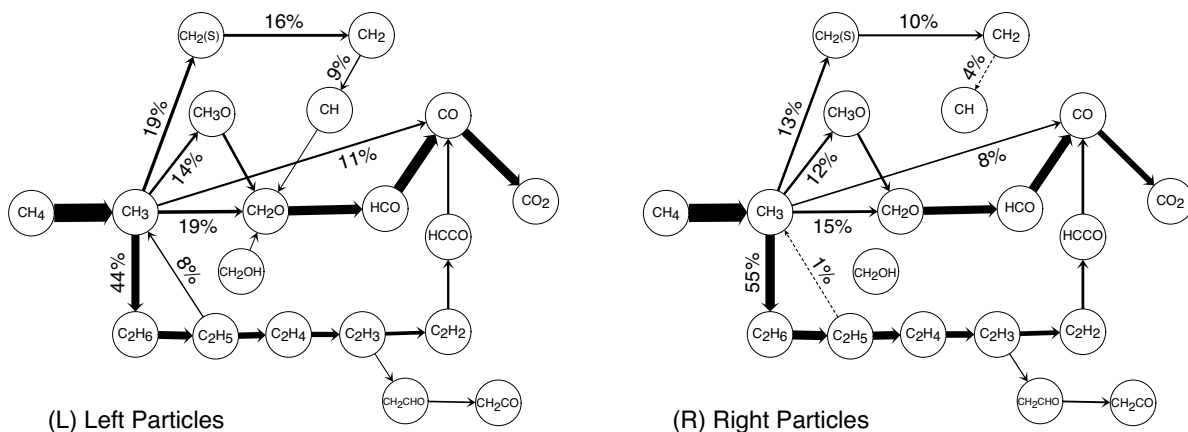

Figure 7: Carbon reaction path diagrams for vortex flame interaction, $\phi = 1.2$. Here only paths of strength $> 5\%$ of the largest path, $CH_4 \rightarrow CH_3$, are shown. For some paths of interest their weights are shown as a percent of the strongest.

in fuel methane molecules and released from the same initial point as the carbon atoms discussed above. For both H and H_2, we examine how far the H-atoms are transported before the molecule reacts. The trajectories show that atomic H exists on average for less than 4 μs, and is therefore too reactive to exist long enough for significant transport by advection or diffusion. The H_2 molecules are considerably longer-lived, and behave quite differently. We find that when H atoms from CH_4 first become part of an H_2 molecule, that molecule exists on average for 0.6 ms on the left but 1.3 ms on the right. In Figure 9 we show pdfs of the total horizontal distance traveled by these H_2 molecules. The symmetric boundary conditions in the computation bias molecules on the left to move right and molecules on the right to move left, since random-walk steps through the boundary are reflected back into the domain. These biases have been removed from the pdf data by keeping
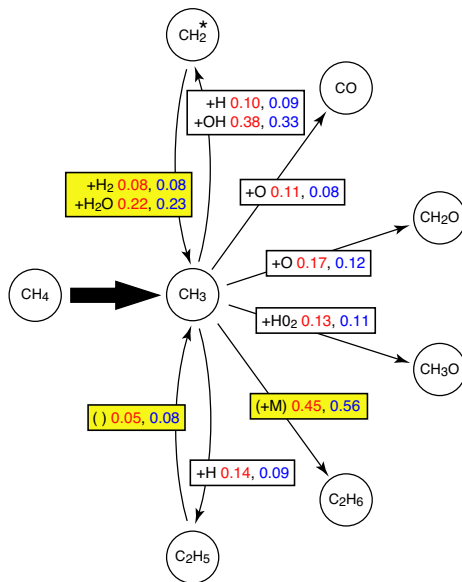
Figure 8: Dominant chemistry of CH_3 in the $\phi = 1.2$ case, determined from stochastic particle analysis. Each pathway is annotated with the associated reaction partner(s) and strength, normalized to the net number of $CH_4 \rightarrow CH_3$ events. The red values represent statistics of particles released on the left, the blue values from particles release on the right. Only paths of strength $> 5\%$ are shown. Pathways not involving radical partners are highlighted yellow, and are increased in the side interacting with the vortex over those in the unperturbed side. All CH_3 destruction reactions involving radicals are weaker in the strained flame region, and in particular paths leading to CH through the $CH_2(s)$ molecule are reduced while those leading to the C_2 branch through C_2H_5 and C_2H_6 are enhanced.

track of the number of steps through the boundary, n_b, and if n_b is odd, mirroring the particle through the relevant boundary to obtain a true final position. A dramatic difference is observed for particles on the right in the strained section of the flame. We observed more than a factor of three difference in mean distance traveled horizontally, showing that H_2 is transported out of the local flame zone by the vortical flow. The reduction in H_2 in the flame zone modifies the chain-branching reactions leading to a reduction in the available radical pool.

The behavior of CH_3O is more subtle. As shown in the reaction path diagram, the changes in the observed CH_3O mole fraction are not caused by shifting of the integrated chemical pathways; the net production of CH_3O on the right hand side is somewhat reduced in both the rich and the lean flames. The computed trajectories show that CH_3O is created by essentially one reaction, $CH_3 + HO_2 \rightarrow CH_3O + OH$. There are two reactions that dominate CH_3O's destruction.[1]

$$Rxn\ 57: \quad CH_3O\,(+\,M) \rightarrow CH_2O + H\,(+\,M)$$
$$Rxn\ 170: \quad CH_3O + O_2 \rightarrow CH_2O + HO_2$$
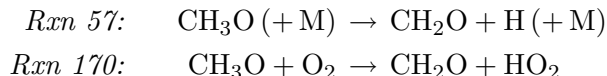
Comparison of these two destruction reaction shows that most of the CH_3O is destroyed by Rxn 57 in both the right and lean cases. However, CH_3O molecules destroyed by Rxn 170 exist on average much longer than those destroyed by Rxn 57. (The time for which a molecule exists is important

---

[1]Reaction numbers are taken from GRI-Mech 3.0 specification of kinetics

because the observed molar concentration is determined by how much of a molecule is produced and how long it exists before reacting again.)

To understand the observed "bloom" in CH_3O as the vortex interacts with the flame we must examine how the destruction reactions change on the right hand side as the flame interacts with the vortex. In both the rich and the lean cases, the relative strengths of the two destruction reactions remains unchanged. However, interaction with the vortex changes the average lifetime of CH_3O. For CH_3O destroyed by Rxn 57, in the rich case the average lifetime increases by 30% while for the lean case it increases by 10%. More dramatically, for CH_3O destroyed by Rxn 170, the lifetime on the right hand side increases by more than 100% for both the rich and lean flames. This increase in longevity, not a shift in the chemical pathways, is responsible for the enhancement of CH_3O during interaction with the vortex. Further examination of the particle trajectories shows that, on average, Rxn 170 occurs at lower temperatures on the right than on the left for both equivalence ratios. This occurs because the temperature profile is steepened on the right due to vortex-induced strain; thus, diffusion transports CH_3O into a cooler region on the right than on the left. Since this reaction is strongly temperature dependent ($\sim T^{7.6}$), CH_3O particles survive longer on average before reacting.

Thus, the behavior of the two species, CH and CH_3O represent different types of phenomena. In the case of CH the observed behavior is related to a shift in the observed chemical pathways. For CH_3O, the observed behavior arises from a change in the timing of production and destruction of the molecule.

3.3 Laminar Diffusion Flame

The final example focuses on the nitrogen chemistry in a cylindrically-symmetric laminar diffusion flame. For this example, the flame is modeled using a reaction mechanism of Glarborg et al. [17]. This mechanism, which includes detailed nitrogen chemistry, contains 65 species and 447 reactions. The case we consider here was part of a combined experimental and numerical study of the effect of fuel-bound nitrogen in the form of NH_3 on NO_x formation [4, 36]. Here we consider
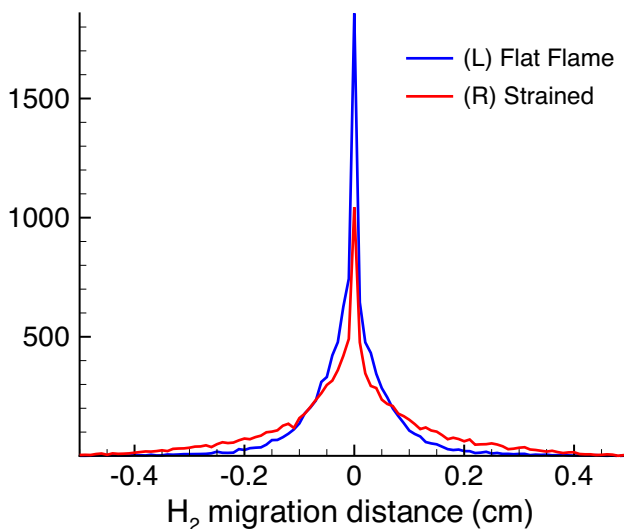

Figure 9: Symmeterized distributions of horizontal H_2 migration show how the flowfield strain disrupts local hydrogen chemistry in the rich flame.

12

only the case with no added NH_3. Temperature and NO mole fraction obtained from the continuum solution are shown in Figure 10.
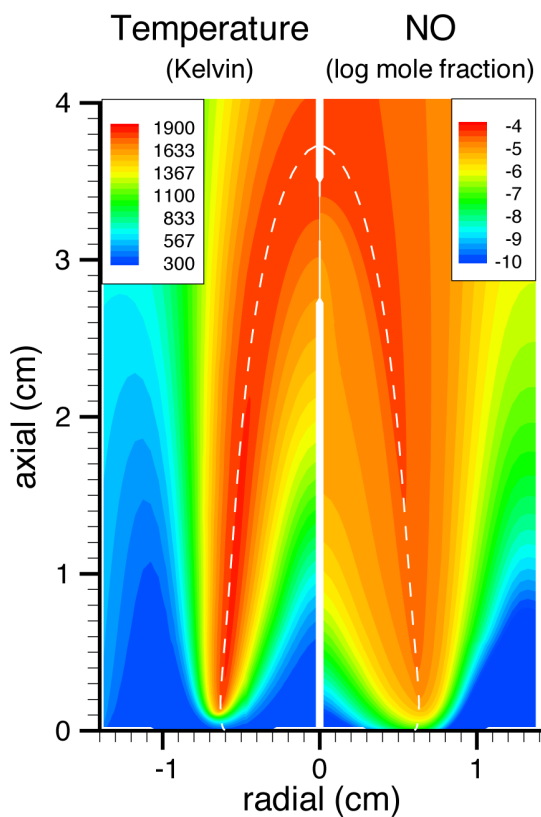

Figure 10: Temperature and NO mole fraction for the laminar nonpremixed flame. The dotted white line is the stoichiometric boundary between the fuel and air.

An important scientific objective in studying these types of flames is to study the formation of NO. For the case we are considering the only source of nitrogen is N_2 in both the fuel and the oxidizer streams. Because N_2 is a relatively stable molecule, only 26 ppm of NO is formed, so the number of trajectories in which reactions occur is very small; we are essentially looking for rare events. Although we can examine NO chemistry as before by sampling N in N_2 molecules entering the domain, we would require a large number of trajectories to obtain a statistically significant set of reacting trajectories. Alternatively, we can *a priori* decide to look only at "interesting" trajectories; i.e., trajectories where N_2 reacts. This is done by using the continuum reaction rates for N_2 over the domain to construct a probability distribution that reflects where N_2 will first react. We use one random variable to sample this distribution for points in space at which to begin the trajectories, and then we use a second random variable to sample the distribution of N_2 reactions at such points for the initiating reactions. This type of procedure is inspired by stochastic models for studying rare reaction phenomena in biological models originally developed by Gillespie [14, 15]. We simulate 10^6 trajectories for the N atom, beginning with the initial breakup of N_2. With this approach to sampling rare events, approximately 5% of the paths result in NO, reducing by a factor of about 2000 the total number of trajectories required to understand those producing the 26 ppm of NO. We use the particle trajectories to compute a net reaction path diagram for the nitrogen

chemistry which is presented in Figure 11. As in the steady premixed flame case, we can compute the analogous net reaction graph from the continuum data and the results show that the nitrogen chemistry as represented by the particles agrees with the analytic rate integration to within a few percent on all paths.
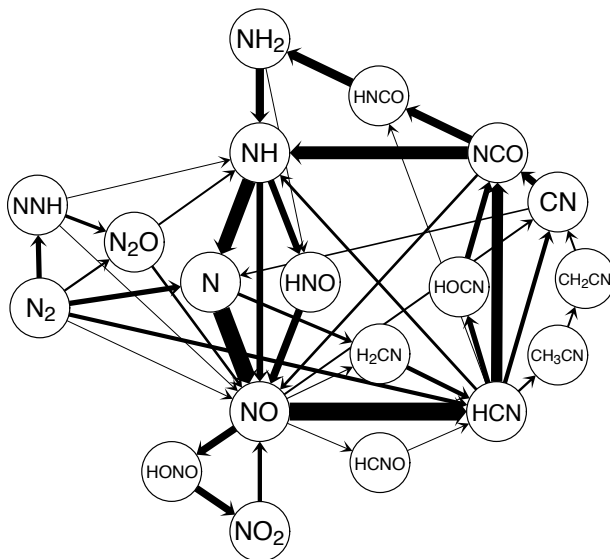

Figure 11: Reaction path diagram for nitrogen chemistry. Only edges at least 3% of the strongest are shown.

We now demonstrate that stochastic particles can also recover the spatial structure of the continuum solution. Assume that we are given a lattice that covers the computational domain. For each cell in the lattice and for each trajectory that crosses that cell, we determine the residence time of N while it is part of an NO molecule in that cell. If we sum these residence times over an ensemble of trajectories the result is proportional to the molar concentration of NO. In Figure 12, we show the NO profile, weighted by local radius (this scaling is necessary since the the residence time is in units proportional to moles/lattice cell not moles/volume.) Even for a modest number of particles the residence time provides a reasonable, if somewhat ephemeral, view of the concentration profile. As the number of samples is increased, however, the agreement becomes increasingly good. We also note that better agreement can be obtained with fewer trajectories if we use a coarser lattice.

These examples show that the stochastic particle approach is able to recover both the chemical and spatial structure of the flame even for NO_x chemistry where the net NO_x effluent is approximately 26 ppm. As a final illustration of the use to stochastic particles, we examine an issue for these types of flames that is not easily determined from the continuum solution. To pose the question, we consider the nitrogen reaction path analysis for this flame presented in Figure 11. The N in nitrogen oxides leaving the system enters the system as N_2 which is broken into N, NNH, HCN, etc. and eventually exits the domain as either NO, or NO_2. The path diagram shows a loop in which nitrogen atoms reside for a time in carbon species. Indeed, the flow through some carbon species is greater than that out of N_2. This indicates that cyano chemistry plays an important role in the formation of NO_x with an N atom possibly recycling through the carbon species multiple times before exiting the domain in NO_x.

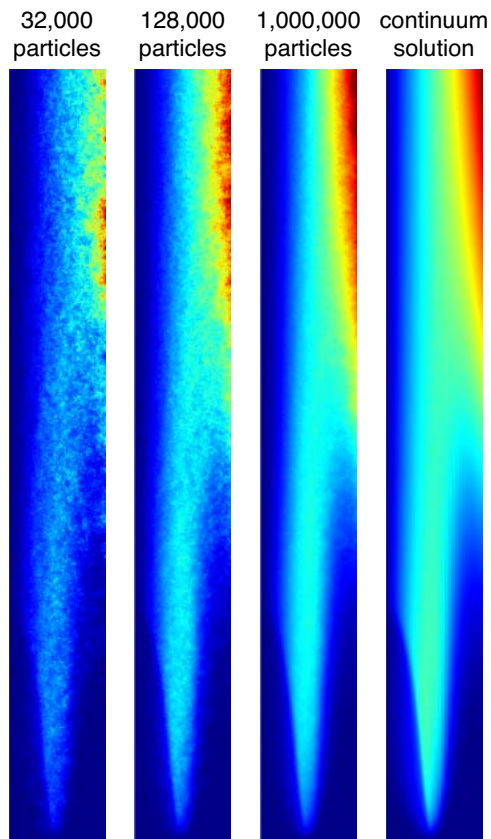To understand the role of this carbon recycling on NO_x chemistry we examine the trajectories

Figure 12: NO concentration in moles/area comparing 32,000, 128,000 and 1,000,000 particles with the continuum solution.

used to compute Figure 11's nitrogen reaction path diagram and extract the subset of those paths that exit the domain as NO or NO_2. For each of these trajectories, we calculate the number of times the N atom we are tracking changes from a non-carbon containing species to a carbon species, and refer to this quantity as the number of cycles for that trajectory. We can then compute a probability distribution for the number of carbon recycling cycles undergone by NO and NO_x molecules leaving the system. The resulting data, presented in Figure 13, are well approximated by the discrete geometric probability distribution

$$P(n) = \lambda(1 - \lambda)^n \quad \text{for } \lambda = 0.33$$

indicating that entering the recycling loop can be modeled as the arrival time for a Bernoulli process.

We can also use the particle trajectories to quantify the spatial structure of the recycling behavior. In Figure 14 we plot the initial reaction location for each particle that exits the domain as NO or NO_2, colored by the number of times it will cycle through cyano species before leaving. We can see that particles that initially react on the outer edge of the flame are not affected by carbon recycling. However, considerable carbon recycling occurs for trajectories initiating on the rich side of the flame sheet, and it becomes increasingly important as we approach the base of the flame. This provides some quantification of the overall behavior of the system and allows us to obtain a spatial picture that indicates where carbon chemistry plays an important role in NO_x formation.
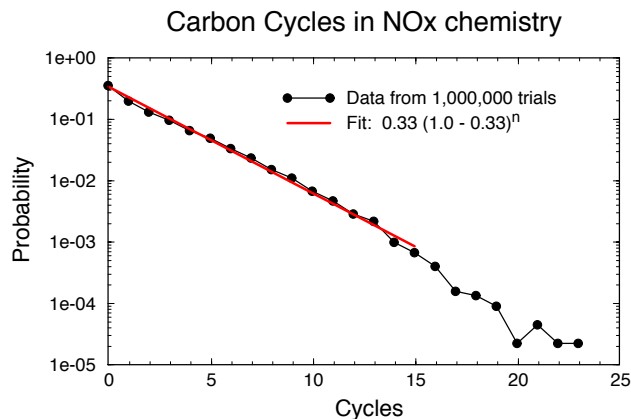
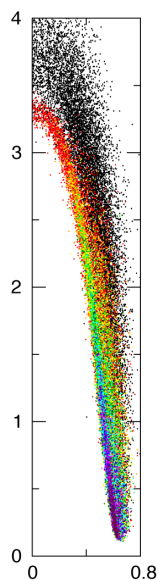Figure 13: Distribution of carbon cycles in NO_x chemistry.

Figure 14: Location of initial reaction for exiting NO_x particles. Black points mark initial reaction locations for particles that do not participate in carbon recycling. The remaining points are color-coded to indicate the number of carbon cycles in the particle history using a rainbow palette ranging from red ($= 1$) to violet (≥ 12).

4   Summary and Conclusions

We have developed a new diagnostic methodology for analyzing combustion simulations. This approach is based on tracking atoms through the system using a stochastic particle formulation that models advective transport, differential diffusion and reactions using the results of a pre-existing solution to the reacting flow equations. We have demonstrated that the method can recover key properties of the continuum solution and provides a mechanism for diagnosing the behavior of complex reacting flows. Perhaps one of the most intriguing properties of this approach is that is allows questions about the reactions and transport to be posed in a natural and straightforward

16

manner. The method has been implemented for multidimensional time-dependent flows and can directly utilize the hierarchical grid system generated by our block-structured adaptive reacting flow algorithm. Our long term goal is to use the stochastic particle approach to study chemical behavior in three-dimensional, time-dependent turbulent combustion.

A   Appendix. Chemical Reactions as Markov Processes

In a Markov process the probability of transition from one state to another depends only on the current state. Representing the movements of atoms among molecules as a Markov process must address three issues: large-rate reversible reactions, reaction ambiguities, and molecules with multiple atoms of the same kind.

A.1   Reversible Reactions

The transition probabilities for the chemical Markov process represent reactions most of which are reversible. The forward and reverse rates either can be treated separately or can be coalesced into a single net destruction (or creation) rate. Since creation rates do not enter the construction of transition probabilities explicitly, the choice makes a substantial difference in the behavior of our algorithm. In Figure 15, we consider the situation of large forward and backward reaction rates that are near equilibrium. If the destruction probability for species M_1 involved the coalesced rate, the net probability of transferring A from M_1 to M_2 would be very small, and atoms entering molecule M_1 will nearly always transform to M_3. However, in reality, the atom bounces back and forth from M_1 to M_2 and is equally likely to transform to M_4 as M_3. To capture this behavior, both forward and reverse version of each the reversible reactions must be taken into account when constructing the destruction probabilities. In this way, it is possible for a traced atom to make several jumps between host molecules over the time interval Δt since $\Delta t_c < \Delta t$. Note that in opting not to coalesce the forward and reverse rates, our algorithm incurs a more restrictive Δt_c.
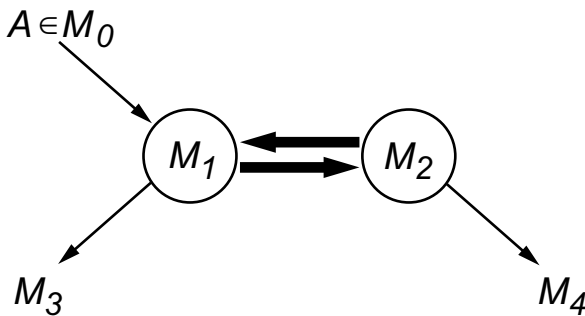

Figure 15: Two species (M_1 and M_2) with rapid forward and backward reactions near equilibrium. If tracked particle $A \in M_0$ enters the M_1 species group, the probability that A will emerge later in the M_4 group depends on whether the production rates between M_1 and M_2 are coalesced.

A.2   Reaction ambiguities

There are several subtleties associated with constructing the Markov process from a reaction kinetics database. A CHEMKIN [24] mechanism file includes very little information about the

atomic details of the reactions. Specifically, there may not be enough information to determine the specific molecule in the product list to which our trace atom in the reactants has been converted. The most common example of this situation in the GRI-Mech 3.0 database used in this study occurs when there are at least two reactant and two product species containing our trace atom, as illustrated in Figure 16. In this case, we are tracing N atoms, and will want to map species on the left to species on the right in order to determine the fate of N. This reaction may involve the transfer of a single O atom, in which case the N in the NO_2 molecule becomes the N in the NO molecule. Alternatively, the reaction may exchange O and C atoms so that the N in the NO_2 becomes the N in the NCO. In rare cases, both options may occur with some finite probability, or the process may even involve more complex intermediate steps. Unique decomposition of the reaction may therefore require intimate knowledge of the molecular bond structures involved and that data is not encoded in the CHEMKIN file.
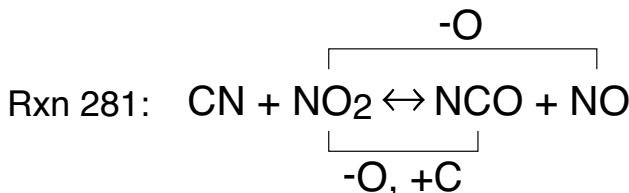

Figure 16: Example of a potentially ambiguous reaction. The CHEMKIN specification does not indicate whether this reaction simply exchanges an O atom from NO_2 to the CN molecule or if it represents a multi-step exchange event.

In our implementation, we have arbitrarily resolved such ambiguities with a simple set of "rules" to apply to the reaction decomposition. The rules are motivated by a knowledge of molecular processes in consultation with P. Glarborg [16]. We summarize the rules as follows.

- Rather than exchange-type processes, we prefer simple shuffling reactions that transfer a single atom or element group from one base molecule to another.

- We prefer shuffling the smallest group of atoms (in number first, then by atomic weight).

- We avoid the transfer of single carbon atoms, or cases that break C-O bonds.

The rudimentary rules may well be incorrect for some reactions in the GRI-Mech 3.0 mechanism. We note, however, that the resolution of these special cases has very little impact on the chemical analyses presented in this paper. The issue is generic to the stochastic particle analysis approach, and new applications should be approached with care.

A.3 Multiple atoms per molecule

Once the details of the reactions have been determined, the only additional issues concern molecules that contains more than one atom of element A. If the molecule is symmetric with respect to A, we can assign probabilities for the destination molecule based on simple counting arguments and a uniform distribution. This case is illustrated in Figure 17a which considers the behavior of H in the reaction $O + CH_4 \rightleftharpoons OH + CH_3$. If we assume that this reaction occurs, then there is a 25% chance the H atom will be shifted to the OH radical and a 75% chance that it will be shifted to CH_3. Thus, in defining $\mathfrak{M}$, if p is the probability of the reaction occurring, then we

specify that $0.25p$ is the probability of the transition $CH_4 \to OH$ and $0.75p$ is the probability of the transition $CH_4 \to CH_3$.

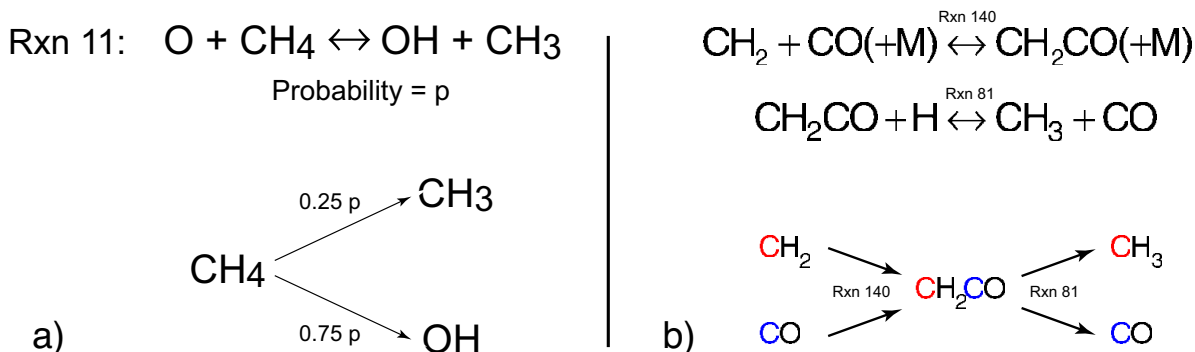Figure 17: Examples of reactions involving molecules with several of the atoms being tracked. Example a) shows a symmetric case involving H atoms in CH_4. Example b) show an unsymmetrical case involving carbon.

When the structure of M is asymmetric with respect to the A atoms, we need to know which position (up to symmetry) A occupies; and we must augment the definition of the states and the reaction probabilities to reflect this location (eg. to prevent physically impossible transitions). In Figure 17b we show an example of an asymmetric molecule participating in reactions that illustrate the issues. Here, two carbon-containing species react to form a single composite molecule which subsequently breaks apart. After the second reaction, we see that the carbon atom originally in the CH_2 molecule becomes the carbon atom in CH_3; physically, it cannot be the carbon atom from the CO molecule. For the reaction history to be correct, this positional information needs to be included in the definition of $\mathfrak{M}$. In order to include this information and preserve the Markov property of $\mathfrak{M}$, the two different carbon positions in CH_2CO need to be represented as distinct states with their own transition properties. We note that in the present implementation, we have not distinguished these states and have used the treatment discussed above for symmetric molecules. For the flames considered here, no reactions involving asymmetric molecules played any substantive role in the dynamics; however, if more complex fuels were considered this type of effect could become important.

Acknowledgment

References

[1] M. Baum, T. J. Poinsot, D. C. Haworth, and N. Darabiha. Direct numerical simulation of $H_2/O_2/N_2$ flames with complex chemistry in two-dimensional turbulent flows. *J. Fluid Mech.*, 281:1–32, 1994.

[2] J. B. Bell, N. J. Brown, M. S. Day, M. Frenklach, J. F. Grcar, and S. R. Tonse. The dependence of chemistry on the inlet equivalence ratio in vortex-flame interactions. *Proc. Combust. Inst.*, 28:1933–1939, 2000.

[3] J. B. Bell, M. S. Day, and J. F. Grcar. Numerical simulation of premixed turbulent methane combustion. *Proc. Combust. Inst.*, 29:1987–1993, 2002.

[4] J. B. Bell, M. S. Day, J. F. Grcar, W. G. Bessler, C. Schultz, P. Glarborg, and A. D. Jensen. Detailed modeling and laser-induced fluorescence imaging of nitric oxide in a NH_3-seeded non-premixed methane/air flame. *Proc. Combust. Inst.*, 29:2195–2202, 2002.

[5] J. B. Bell, M. S. Day, I. G. Shepherd, M. Johnson, R. K. Cheng, V. E. Beckner, M. J. Lijewski, and J. F. Grcar. Numerical simulation of a laboratory-scale turbulent V-flame. Technical Report LBNL-54198, Lawrence Berkeley National Laboratory, Berkeley, 2003. Submitted for publication.

[6] B. A. V. Bennett, C. S. McEnally, L. D. Pfefferle, and M. D. Smooke. Computational and experimental study of axisymmetric coflow partially premixed methane/air flames. *Combust. Flame*, 123:522–546, 2000.

[7] J. H. Chen and H. Im. Correlation of flame speed with stretch in turbulent premixed methane/air flames. *Proc. Combust. Inst.*, 27:819–826, 1998.

[8] M. S. Day and J. B. Bell. Numerical simulation of laminar reacting flows with complex chemistry. *Combust. Theory Modelling*, 4:535–556, 2000.

[9] T. Echekki and J. H. Chen. Direct numerical simulation of autoignition in non-homogeneous hydrogen-air mixtures. *Combust. Flame*, 134:169–191, 2003.

[10] A. Ern, C. C. Douglas, and M. D. Smooke. Detailed chemistry modeling of laminar diffusion flames on parallel computers. *Int. J. Sup. App.*, 9:167–186, 1995.

[11] M. Frenklach, H. Wang, M. Goldenberg, G. P. Smith, D. M. Golden, C. T. Bowman, R. K. Hanson, W. C. Gardiner, and V. Lissianski. GRI-Mech—an optimized detailed chemical reaction mechanism for methane combustion. Technical Report GRI-95/0058, Gas Research Institute, 1995. http://www.me.berkeley.edu/gri_mech/.

[12] B. Fryxell, K. Olson, P. Ricker, F. X. Timmes, M. Zingale, D. Q. Lamb, P. MacNeice, R. Rosner, J. W. Truran, and H. Tufo. FLASH: An adaptive mesh hydrodynamics code for modeling astrophysical thermonuclear flashes. *Astrophys. J. Suppl. S.*, 131:273–334, 2000.

[13] W. C. Gardiner, Jr. The pc, pr, pm, and ps method of formulating the results of computer modeling studies of chemical reactions. *The Journal of Computational Chemistry*, 81:2367–2371, 1977.

[14] D. T. Gillespie. Stochastic simulation of chemical processes. *J. Comput. Phys.*, 22:403, 1976.

[15] D. T. Gillespie. Exact stochastic simulation of coupled chemical reactions. *J. Phys. Chem.*, 81:2340–2361, 1977.

[16] P. Glarborg. Private communication, 2004.

[17] P. Glarborg, P. G. Kristensen, K. Dam-Johansen, M. U. Alzueta, A. Millera, and R. Bilbao. Nitric oxide reduction by non-hydrocarbon fuels. Implications for reburning with gasification gases. *Energy Fuels*, 14:828–838, 2000.

[18] I. Glassman. *Combustion.* Academic Press, third edition, 1996.

[19] J. F. Grcar, P. Glarborg, J. B. Bell, M. S. Day, A. Loren, and A. D. Jensen. Effects of mixing on ammonia oxidation in combustion environments at intermediate temperatures. *Proc. Combust. Inst.*, 2004. To appear.

[20] D. C. Haworth, R. J. Blint, B. Cuenot, and T. J. Poinsot. Numerical simulation of turbulent propane-air combustion with nonhomogeneous reactants. *Combust. Flame*, 121:395–417, 2000.

[21] R. Hilbert, F. Tap, H. El-Rabii, and D. Thévenin. Impact of detailed chemistry and transport models on turbulent combustion simulations. *Prog. Energy Combust. Sci.*, pages 61–117, 2004.

[22] M. Hilka, D. Veynante, M. Baum, and T. J. Poinsot. Simulations of flame-vortex interactions using detailed and reduced chemical kinetics. In *Symposium on Turbulent Shear Flows*, volume 10, pages 19.19–24, Pennsylvania State University, 1995.

[23] R. J. Kee, J. F. Grcar, M. D. Smooke, and J. A. Miller. PREMIX: A fortran program for modeling steady, laminar, one-dimensional premixed flames. Sandia National Laboratories Report SAND85-8240, Sandia National Laboratories, Livermore, 1983.

[24] R. J. Kee, R. M. Ruply, E. Meeks, and J. A. Miller. Chemkin-III: A FORTRAN chemical kinetics package for the analysis of gas-phase chemical and plasma kinetics. Sandia National Laboratories Report SAND96-8216, Sandia National Laboratories, Livermore, 1996.

[25] Y. Mizobuchi, S. Tachibana, J. Shinio, S. Ogawa, and T. Takeno. A numerical analysis of the structure of a turbulent hydrogen jet lifted flame. *Proc. Combust. Inst.*, 29:2009–2015, 2002.

[26] R. H. Mohammed, M. A. Tanoff, M. D. Smooke, and A. M. Schaffer. Computational and experimental study of a forced, time-varying, axisymmetric, laminar diffusion flame. *Proc. Combust. Inst.*, 27:693–702, 1998.

[27] H. N. Najm, O. M. Knio, P. H. Paul, and P. S. Wyckoff. A study of flame observables in premixed methane-air flames. *Combust. Sci. Technol.*, 140:369–403, 1998.

[28] H. N. Najm, P. H. Paul, C. J. Mueller, and P. S. Wyckoff. On the adequacy of certain experimental observables as measurements of flame burning rate. *Combust. Flame*, 113(3):312–332, 1998.

[29] H. N. Najm and P. S. Wyckoff. Premixed flame response to unsteady strain rate and curvature. *Combust. Flame*, 110(1–2):92–112, 1997.

[30] Q.-V. Nguyen and P. H. Paul. The time evolution of a vortex-flame interaction observed via planar imaging of CH and OH. *Proc. Combust. Inst.*, 26:357–364, 1996.

[31] J.-M. Samaniego. Stretch-induced quenching in flame-vortex interactions. In *1993 Annual Research Briefs*, page 205. Center for Turbulence Research, Stanford University.

[32] M. D. Smooke, A. Ern, M. A. Tanoff, B. A. Valdati, R. K. Mohammed, D. F. Marran, and M. B. Long. Computational and experimental study of NO in an axisymmetric laminar diffusion flame. *Proc. Combust. Inst.*, 26:2161–2170, 1996.

[33] M. D. Smooke, P. Lin, J. K. Lam, and M. B. Long. Computational and experimental study of a laminar axisymmetric methane-air diffusion flame. *Proc. Combust. Inst.*, 23:575–582, 1990.

[34] M. D. Smooke, R. E. Mitchell, and D. E. Keyes. Numerical solution of two-dimensional axisymmetric laminar diffusion flames. *Combust. Sci. Tech.*, 67:85–122, 1989.

[35] M. D. Smooke, Y. Xu, R. M. Zurn, P. Lin, J. H. Frank, and M. B. Long. Computational and experimental study of OH and CH radicals in axisymmetric laminar diffusion flames. In *Proc. Combust. Inst.*, volume 24, pages 813–821, 1992.

[36] N. Sullivan, A. Jensen, P. Glarborg, M. S. Day, J. F. Grcar, J. B. Bell, C. Pope, and R. J. Kee. Ammonia conversion and NO_x formation in laminar coflowing nonpremixed methane-air flames. *Combust. Flame*, 131:285–298, 2002.

[37] M. Tanahashi, M. Fujimura, and T. Miyauchi. Coherent fine scale eddies in turbulent premixed flames. *Proc. Combust. Inst.*, 28:529–535, 2000.

[38] M. Tanahashi, Y. Nada, Y. Ito, and T. Miyauchi. Local flame structure in the well-stirred reactor regime. *Proc. Combust. Inst.*, 29:2041–2049, 2002.

[39] F. X. Timmes and S. E. Woosley. The conductive propagation of nuclear flames I. degenerate C+O and O+Ne+Mg white dwarfs. *Astrophys. J.*, 396:649–667, 1992.

[40] F. X. Timmes, S. E. Woosley, and R. E. Taam. The conductive propagation of nuclear flames II. flames in C+O and O+Ne+Mg cores. *Astrophys. J.*, 420:348–363, 1994.

[41] N. Tsuboi, S. Katoh, and A. K. Hayashi. Three-dimensional numerical simulations for hydrogen/air detonation: rectangular and diagonal structures. *Proc. Combust. Inst.*, 29:2783–2788, 2003.

[42] L. Vervisch, R. Hauguel, P. Domingo, and M. Rullaud. Three facets of turbulent combustion modelling: DNS of premixed V-flame, LES of lifted nonpremixed flame and RANS of jet-flame. *J. Turbulence*, 5:1–36, 2004.